EUROPEAN ORGANIZATION FOR NUCLEAR RESEARCH

CERN/PS/88-1 (PO)
20 January 1988

THE 6 kA, 10 kV, 100 Hz POWER SUPPLY AND PULSER FOR THE COLLECTING AND FOCUSING SOLENOID OF THE e^-e^+ CONVERTER IN THE CERN LEP PRE-INJECTOR

J.P. Royer and F. Voelker

ABSTRACT

A small pulsed solenoid behind the positron production target collects the emerging particles and matches their trajectory to the acceptance of the 600 MeV linac accelerating structure.

Following a short review of the requirements, the design criteria of the solenoid power supply and pulser are discussed, and the salient technical features of this unconventional equipment are described.

The performance results obtained during commissioning and initial operation are reported.

CONTENTS

List of figures

List of tables

1. INTRODUCTION

The LEP pre-injector (LPI) [1] consists of two linacs, a 200 MeV high-current electron linac (LIL-V) and a 600 MeV lower- current linac (LIL-W), and of the Electron-Positron Accumulator (EPA) ring.

The 200 MeV linac (LIL-V) produces 12 ns electron beam pulses at 100 Hz repetition frequency, equivalent to a current of 2.5 A, with an energy spread of less than 10%.

The radial dimension of the electron beam hitting the target is 1 to 2 mm and its nominal mean power is ~ 0.6 kW.

The positrons are produced in a 5 mm diameter cylindrical tungsten target, 2 radiation lengths thick (~ 7 mm), with a flat distribution in energy around 8 MeV, within a radius of ~ 1 mm (80% of the particles) and a mean angle of ~ 20°. The e^+/e^- conversion efficiency is ~ 4×10^{-3} at 200 MeV electron incident energy.

The cylindrical target is inserted and brazed in a water-cooled copper block.

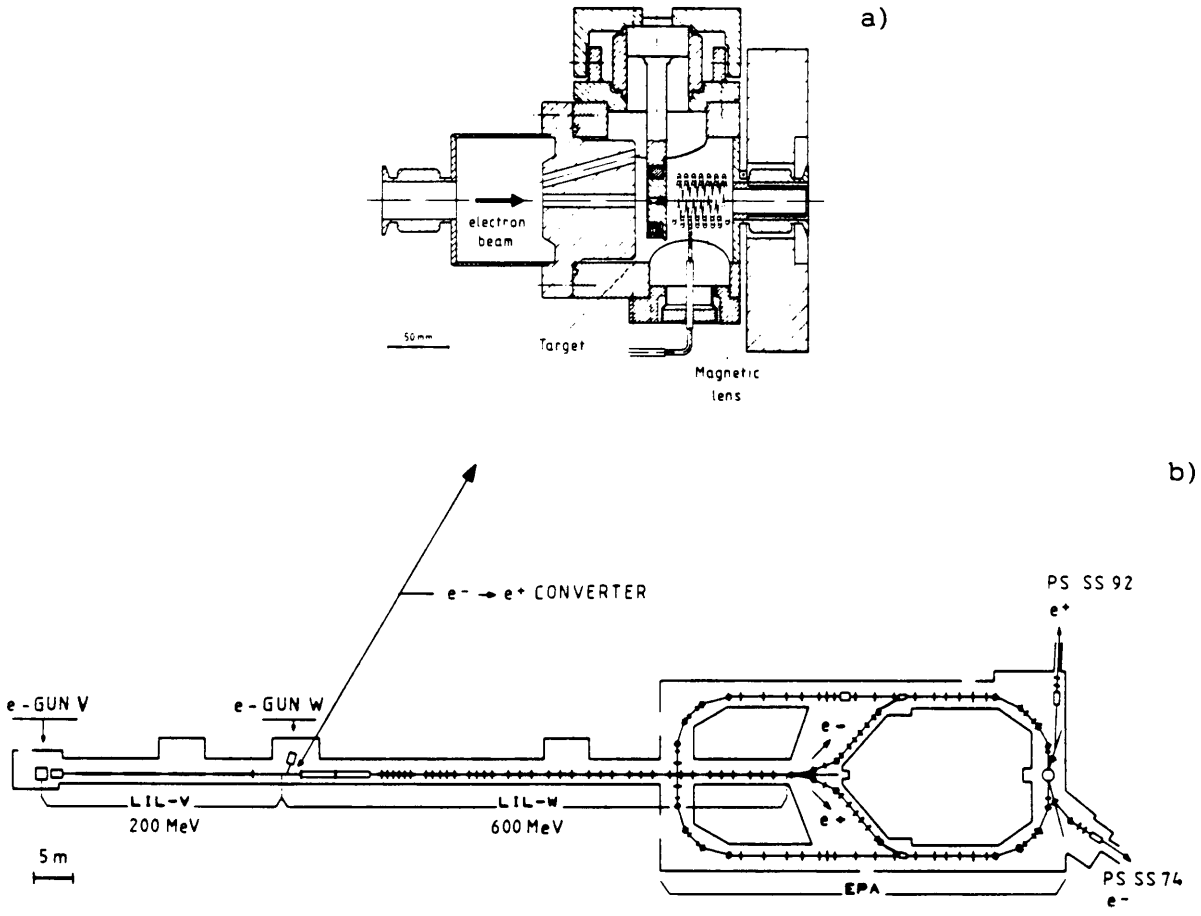

Fig. 1 Electron-positron converter:
a) target and magnetic collecting lens;
b) position of the converter in the LEP preinjector.

Matching of the positrons into the acceptance of the accelerating sections is made by converting the beam of small radius and large divergence (e.g. 2 mm x 160 mrad), to one of larger radius and smaller divergence (8 mm x 40 mrad).

A pulsed solenoid immediately after the target, shown in Fig. 1, is used as an adapting magnetic lens with short focal distance, which contributes to an increase by a factor of ~ 3 of the flux of positrons entering the LIL-W accelerating structure.

The main parameters of the pulsed solenoid are collected in Table 1.

Table 1

Main pulsed solenoid parameters

Physical length	(mm)	48
External/internal diameter	(mm)	45/25
Number of turns/layers		14/2
External/internal diameter of copper tube conductor	(mm)	4/2
Inductance	(μH)	3
d.c. resistance/50 kHz resistance at 20° C	(mΩ)	4/18
Maximum nominal effective current	(A)	135
Peak nominal pulse current	(kA)	6
Maximum average electrical losses	(W)	330
Peak magnetic induction on axis at 6 kA	(T)	1.8
Distance from target block	(mm)	5
Radiation dose rate at 1 m during e^+ production [2]	(Sv/h)	60
Flow of demineralized cooling water	(l/min)	1.2

2. PERFORMANCE REQUIREMENTS

The performance requirements of the pulse generator of the converter solenoid are collected in Table 2.

The power supply shown in Fig. 2 is located in the LPI klystron gallery and consists of a 10 kV charging section (including the electronics and computer interface) as well as of the pulse generator section.

Table 2

Performance requirements

Nominal sinusoidal pulse current into a 4 μH load	(kA)	6
Half-period pulse duration	(μs)	≤ 10
Regular pulse repetition frequency	(Hz)	100
Capacitor charging voltage	(kV)	≤ 10
Voltage recovery after the current pulse	(%)	> 50
Current pulse-to-pulse reproducibility at 100 Hz	(%)	< 1
Cable distance between pulser and load	(m)	~ 10
Possibility to operate at lower pulse repetition frequency		yes
Protection against thyratron failures without interrupting operation		yes
Standard computer control interface		yes
Standard timing sequence (FW, W, ST, and M pulses)		yes

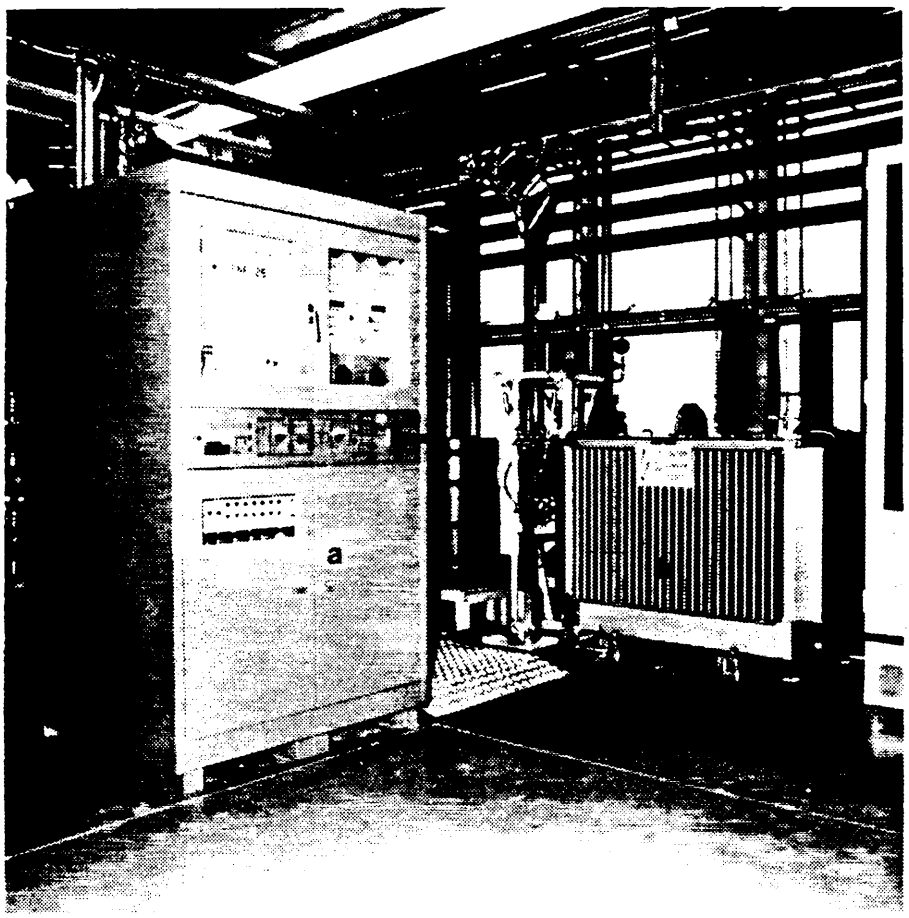

Fig. 2 Collector solenoid power supply:
a) charging section;
b) pulse generator section.

3. CIRCUIT DESCRIPTION AND MODE OF OPERATION

The circuit diagram of the power supply is shown in Fig. 3a, while its mode of operation, is illustrated in Fig. 3b and treated in Appendix B. The parameters of the main components of the power circuit are given in Table 3.

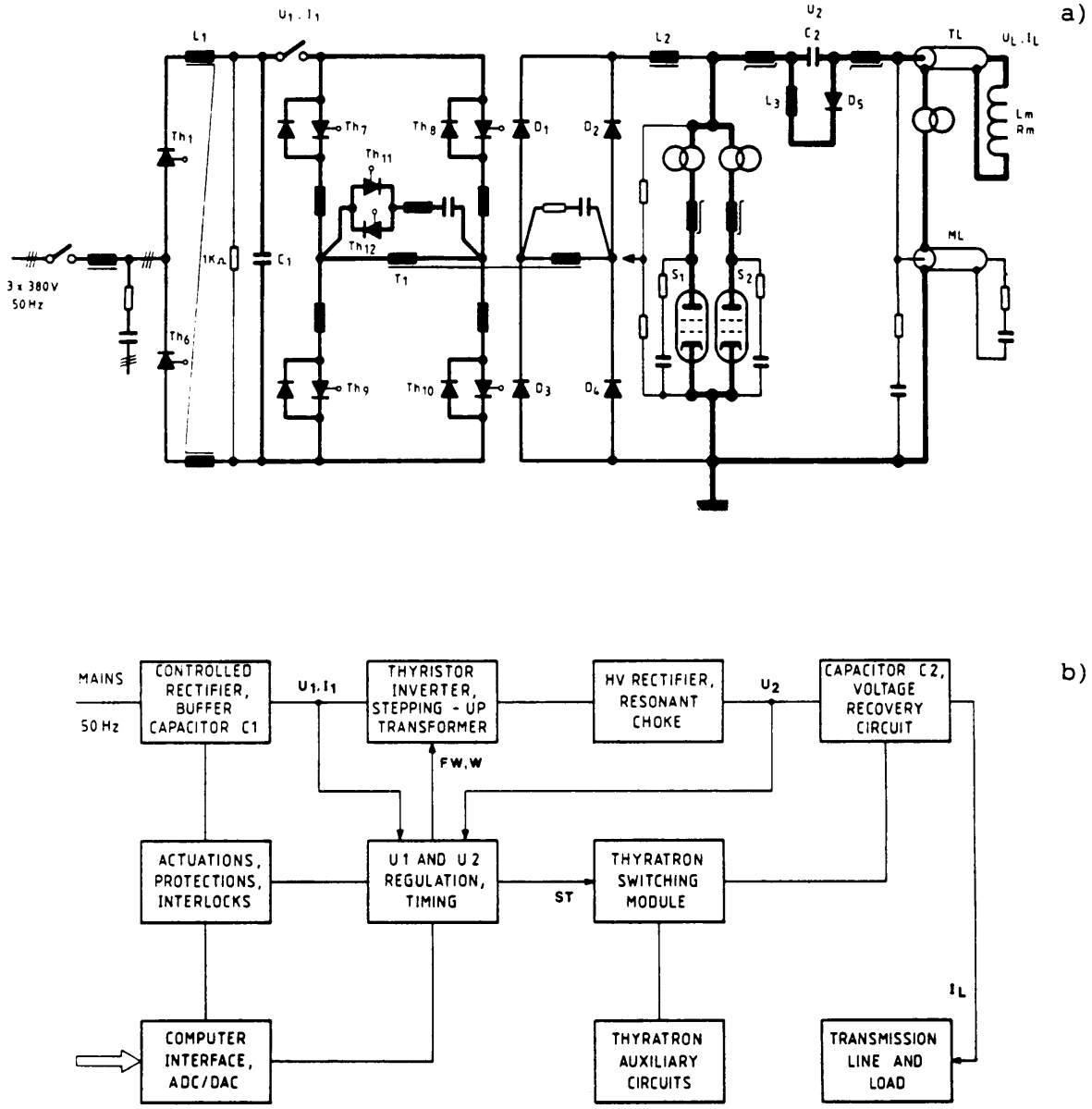

Fig. 3 a) Schematic circuit diagram and,
b) functional block diagram of the power supply.

Table 3

Main circuit parameters

Six-pulse bridge thyristors (Semikron, CH)	Type SKKT 41-16E
Smoothing choke L_1 (mH;mΩ;A)	12.5; 140; 35
Buffer capacitor C_1 (mF;V;kJ)	25; 300; 1.15
Inverter thyristors and diodes (AEG, D)	Type TT 42F 1000
Stepping-up transformer T_1 [U_2(V)/U_1(V);I_2(A)]	9000/300; 1.1
HV rectifier diodes (MEDL, UK)	Type HTZ 12F
Resonant charging choke L_2 (H;Ω;Â)	3 to 4; 8; 2
Thyratron switch S_1,S_2 (EEV, UK)	Type CX1126S
HV energy storage capacitor C_2 (μF;kV;kJ)	2.5; 10; 0.125
Voltage recovery air choke L_3 (mH;mΩ;A)	4; 90; 31
Voltage recovery diodes (BBC, CH)	Type DSA 42-16A
Transmission line TL	10 x RG 213
Current measuring transformers (Pearson, USA)	Type 110 and 1023

The voltage of capacitor C_1 is kept at a preselected value between 50 and 300 V by means of a thyristor rectifier Th_1-Th_6. By firing alternatively opposite pairs of thyristors in the forced-commutated inverter bridge (Th_7-Th_{10} or Th_8-Th_9) the voltage U_{10} at C_1 is applied to the primary of the 1:30 stepping-up transformer T_1. Consequently a voltage of ~ 30 U_{10} excites, through the HV rectifier (D_1-D_4), the resonant (L_2+L_m) C_2 circuit.

Capacitor C_2 is charged cosinusoidally from an initial voltage U_{20} up to a voltage $U_2 \leq 10$ kV within a time of ~ 9.5 ms by means of a damped sine-wave current of amplitude ≤ 2 A.

When the thyratron switch is fired the anode voltage falls from U_2 to its low arc voltage and the load-end side of C_2 assumes a voltage of $-U_2$ which drives current through L_m. The sinusoidal discharge current through capacitor C_2 into the solenoid inductance L_m has a half-period of ~ 10 μs and a peak value ≤ 6 kA.

At the zero crossing of the load current pulse the unidirectional thyratron normally interrupts the discharge of C_2 when the capacitor has its maximum reverse voltage; consequently the anode voltage jumps within a fraction of a microsecond to a negative voltage of almost $-U_2$ with a du/dt up to 50 kV/μs.

Finally, a resonant voltage recovery circuit D_5, L_3 recharges C_2 to U_{20} within 300 μs.

The waveforms of the thyratron voltage and current, shown in Fig. 4, illustrate the mode of operation of the circuit.

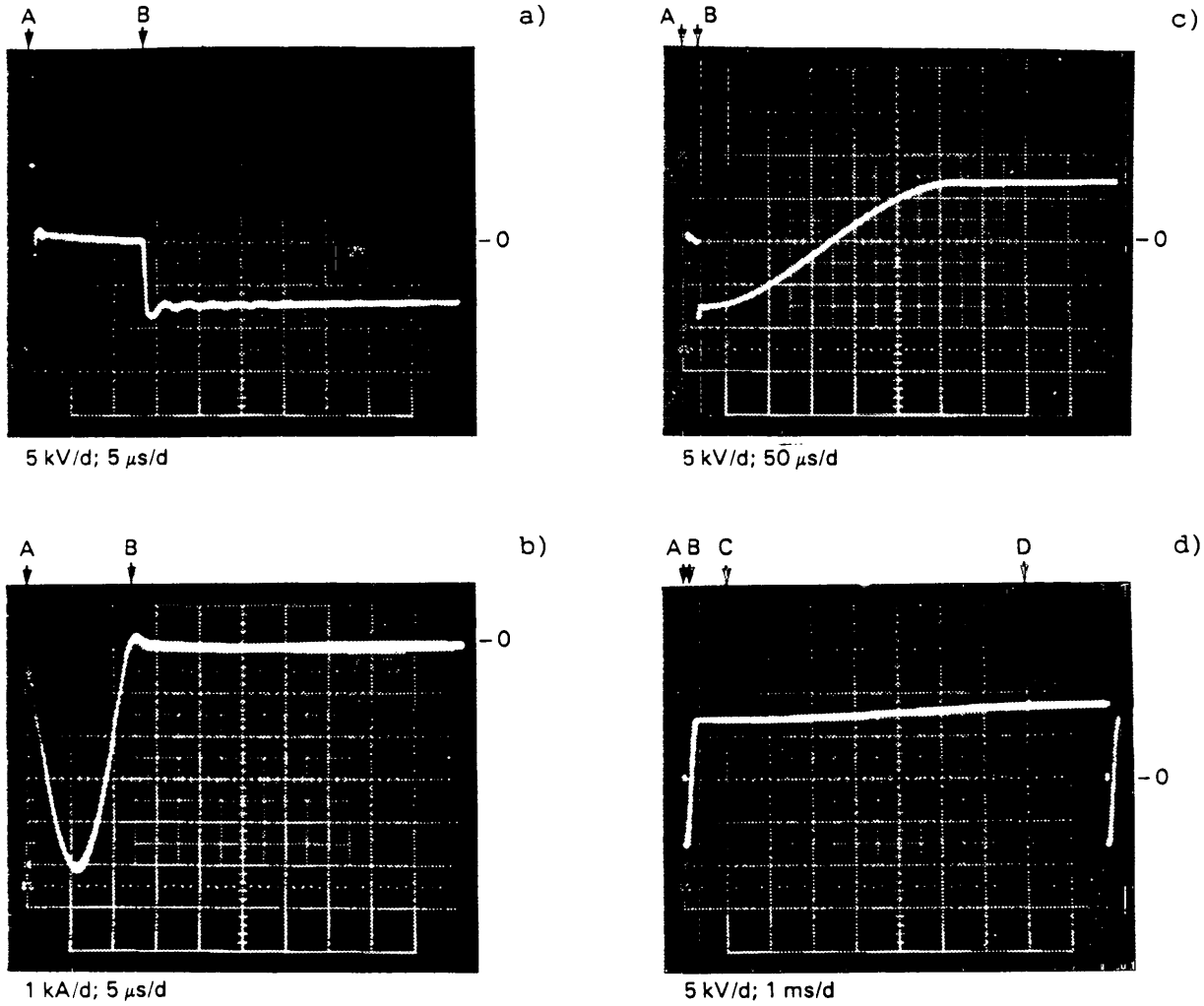

Fig. 4 Waveforms of thyratron voltage and current:
a) voltage during switch on and conduction;
b) current pulse;
c) reverse voltage and voltage recovery at C_2;
d) voltage recovery and recharge of C_2.
(A-B and C-D: start-end of current pulse and of C_2 charging).

With respect to other power supplies developed for a similar application at Frascati (Italy) and DESY (Germany), the CERN solution makes wider use of modern power electronics to obtain some interesting features:

i) The voltage source used to charge resonantly the high-voltage (HV) capacitor C_2 is a low-voltage (LV) electrolytic capacitor bank C_1. The thyristor rectifier feeding C_1 allows soft start and fold-back procedures in order to protect the power supply. Minimum energy is stored on the HV side in order to reduce the consequences of any breakdown.

ii) Owing to the inverter bridge the stepping-up transformer operates in an a.c. mode as a 50 Hz unit. The forced commutation of thyristors Th_7 to Th_{10} opens up the possibility of interrupting the charge of C_2 once the selected voltage is attained. This gives the same high pulse-to-pulse reproducibility as achieved elsewhere by means of a more lossy 'de-Q-ing' circuit. On the other hand, in the case of an overcurrent detected on the primary of the stepping-up transformer the operation of the power circuit can be safely interrupted.

iii) The operational sequences and the internal protection of the power supply have been defined with care in order to make the equipment particularly reliable and user-friendly.

It is worth also mentioning some of the difficulties encountered in the course of the development:

i) The regulation of the voltage at C_1 and the charging current limitation are not trivial, when the possibility of operating in a one-shot mode or at any regular pulse repetition frequency up to 100 Hz is to be granted.

ii) The negative voltage across the thyratron at the end of the forward current pulse may make the tube -- which is still highly ionized -- arc back and cause circuit ringing; the consequences being possible damage to the thyratron electrodes as well as excessive charging current and voltage at C_2.

iii) Voltage spikes and ringing, and in particular multiple reflections along the transmission line, had to be suppressed at various points of the circuit. The electromagnetic interference (EMI) problems with respect to the low-level timing and interface electronics have been quite severe.
Concerning the EMI aspects one should point out that the thyratron cathode has been permanently connected to earth potential for practical reasons and that consequently larger stray capacitances are involved in the modulator operation.
The local reference earth is not particularly good and one has to cope with a large amount of electromagnetic noise in the 5 MHz spectrum.
Particular operational precautions had to be taken and all cables connected to the power supply had to be common-mode filtered by means of suitable ferrite cores with different damping characteristics.

4. POWER COMPONENTS AND ASSEMBLIES

4.1 Thyratron switch

The comparative study and selection of an adequate tube and the search for reliable working conditions were an important part of the power-supply development.

The basic characteristics of the thyratrons initially considered for this application are collected in Table 4.

Table 4

Thyratron characteristics

	Type of thyratron				Key data of our application (single tube)
	EEV CX1525	EEV CX1528 (CX1526S)	EEV CX1549	ITT 8479/KU 275 C	
1. Anode					
Peak forward/inverse voltage in oil (kV)	70/70	40/40	40/40	50/50	10/10
Mean rate of rise of inverse voltage (kV/µs)	0.8	0.6	0.6	0.4	> 1
Peak anode current for a rectangular pulse of duration T (in µs) (kA)	$3.5(\frac{3}{T})^{1/2}$	$5(\frac{3}{T})^{1/2}$	$10(\frac{3}{T})^{1/2}$	$5(\frac{5}{T})^{1/2}$	6 kA for T = 10 µs sinusoidal
Max. average anode current (A)	5	5	15	8	4
r.m.s anode current (A)	125	125	350	200	135
Anode heating factor i.e. (peak forward anode voltage) x (peak anode current) x (pulse repetition rate) (V·A·Hz)	10^{11}	0.7×10^{11}	2×10^{11}	4×10^{11}	6×10^{9}
2. Cathode					
Cathode/reservoir heater voltage (V)	6.3/6.3			6.3/< 6	
Cathode/reservoir heater current (A)	36/5	36/5	90/7	< 70/< 25	
3. Grids					
Grid 1 d.c. priming current (A)	0.1 to 2			not spec.	
Grid 1 d.c. voltage drop (V)	15 to 30			not spec.	
Grid 2 idle drive pulse voltage/rate of rise of voltage [kV/(kV/µs)]	0.6 to 2/> 4			1 to 4/> 3	
Grid 2 drive-pulse duration (µs)	> 1			> 2	
Grid 2 negative bias voltage (V)	≤ -120			not spec.	
Gradient grid	yes	no	no	yes	
4. Dissipation and cooling					
Admissible dissipation (kW)	≤ 1.7	≤ 1.7	≤ 5	not spec.	
Max. ambient temperature (° C)	90	90	90	90	
Cooling medium	oil			air	silicon oil

The CX1528 [manufactured by the English Electric Valve Company, UK (EEV)] is a single-gap modulator-type metal-ceramic tube filled with deuterium; it uses a barium-aluminate-impregnated tungsten dispenser cathode; large gas reservoirs are controlled by temperature-sensitive circuits in the base of the tube.

This tube has a comparatively small plasma volume in the grid 2-anode region, which should provide for lower ion and electron clean-up current and a faster decay-time constant of the plasma. This decay-time depends on the plasma volume and temperature, i.e. on the tube dissipation. Amplitude and rate of rise of the reverse anode voltage greatly contribute to the tube dissipation. Experience shows that different practical steps tend to reduce dissipation and to improve the voltage recovery capability of the tube: e.g. increasing the gas pressure, reducing the $\int i\,dt$ and the di/dt of the current pulse, reducing the reverse- voltage spikes and du/dt, etc.

It has been observed that there is an optimum set of parameters determining the gas pressure for each tube. Reverse-voltage spikes and du/dt are also important regarding the probability of electrode damage, of ion implantation on the anode, and of electron avalanches causing forward voltage breakdown.

The CX1528 has finally been selected as the best device available for our application. Nevertheless serious back-arc difficulties were experienced during circuit development, as shown for a typical case in Figs. 5 and 6a.

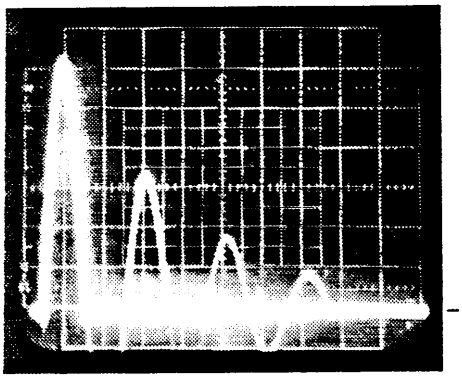

Fig. 5 Thyratron arc-back at the end of anode current pulse.

The tube manufacturer recommends a value of the peak reverse-voltage not exceeding 5 kV during the first 25 µs after current zero crossing and a rate of voltage rise $\leq$ 10 kV/µs. The situation has been improved by adding an RC network in parallel with the tube and a saturating ferrite-core reactor in series with the anode (Figs. 6b and c). By doing so, the first CX1528 tube could be reliably tested up to 6 kA, 100 Hz, in the power-supply prototype. Unfortunately, all other off-the-shelf thyratrons suffered from unacceptable back-arc problems above 4 kA peak anode current.

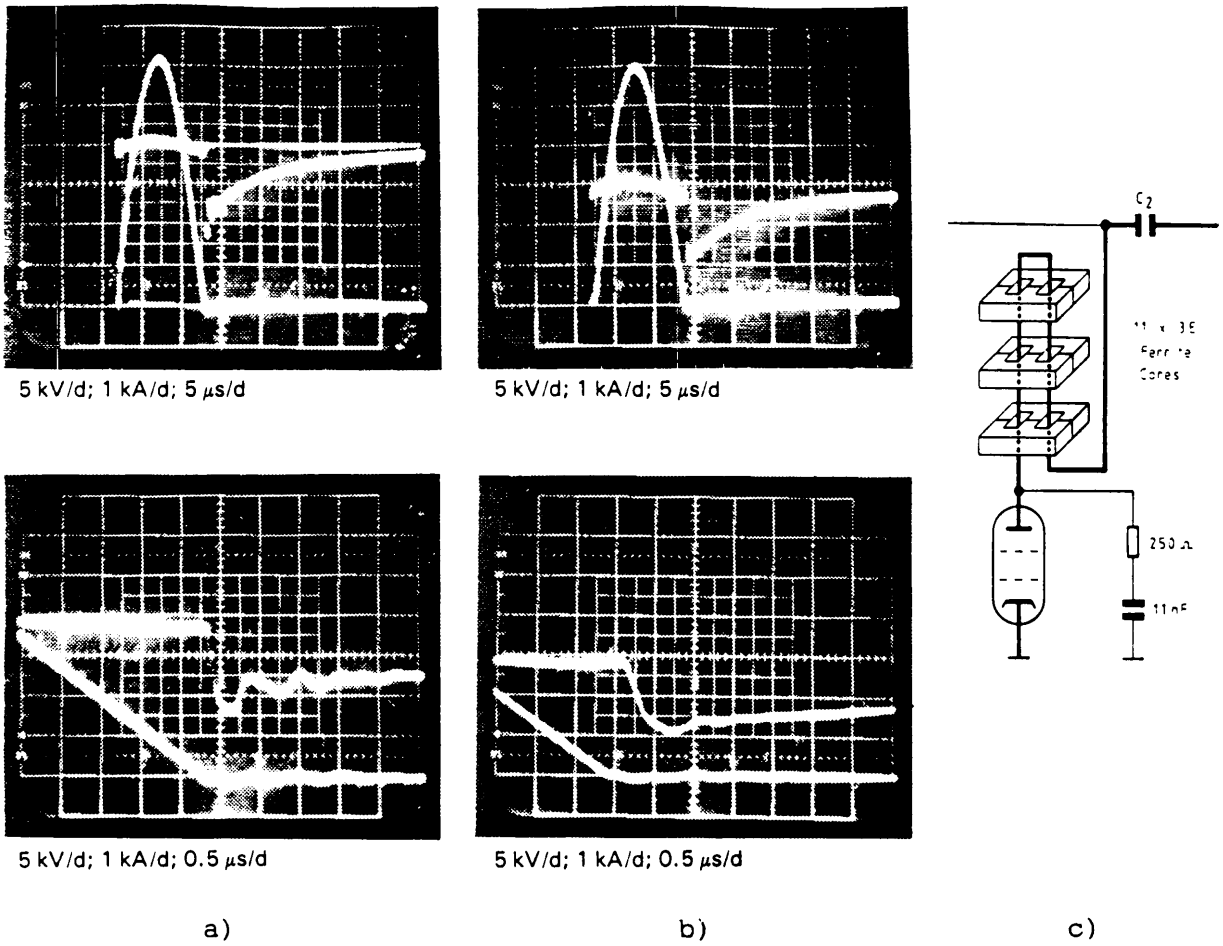

Fig. 6 Waveforms of voltage across the thyratron switch at the end of the 6 kA anode current pulse

a) without and,
b) with the smoothing circuit shown in (c).

Tests done at CERN and at EEV demonstrated that, owing to the lower individual dissipation, peak currents well above 6 kA could be achieved with two tubes connected in parallel. The current sharing can be controlled by means of individual adjustment of the grid 1 voltage. This solution was finally adopted for practical reasons in the course of the project but one can expect that, by further optimization of the operating conditions and by proper shaping of the reverse anode voltage (e.g. suitable RLC network in parallel with the energy storage capacitor C_2) [3], the maximum current capability of a single tube could be substantially increased.

4.2 Thyratron switching module and auxiliary module

These modules are shown in Fig. 7. The switching module, originally conceived for one tube, has been adapted to receive two thyratrons by cutting out the external cylinder wall. The thyratrons

are mounted on an Al base with adequate apertures for cooling-oil circulation. Each thyratron has one multiple connector for its heating and grid 1 bias supplies; the grid 2 bias voltage and the trigger pulse are common to the two tubes. All cabling is done outside the Al cyclinder. A few ferrite rings on the symmetric leads to the anodes provide for decoupling of the parallel connected tubes and for current sharing better than 5%. Current sharing between the tubes is observed to vary slightly from pulse to pulse owing to the residual ripple of the grid 2 bias voltage.

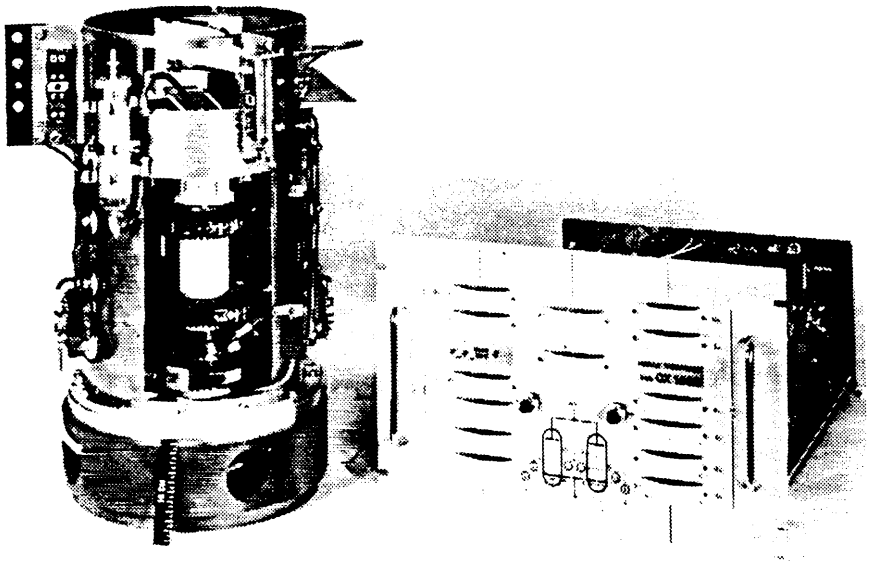

Fig. 7 Thyratron switching module and auxiliary module.

Figure 8 shows a schematic circuit diagram of the auxiliary double-thyratron module.

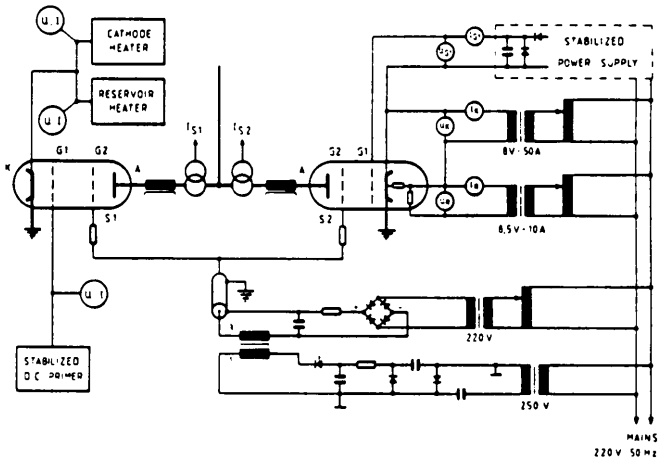

Fig. 8 Schematic circuit diagram of the auxiliary module.

As shown in Fig. 9, current sharing between tubes is optimized by means of separate stabilized grid 1 bias supplies, which permit individual adjustment of the operating point, and by means of a high trigger voltage on grid 2.

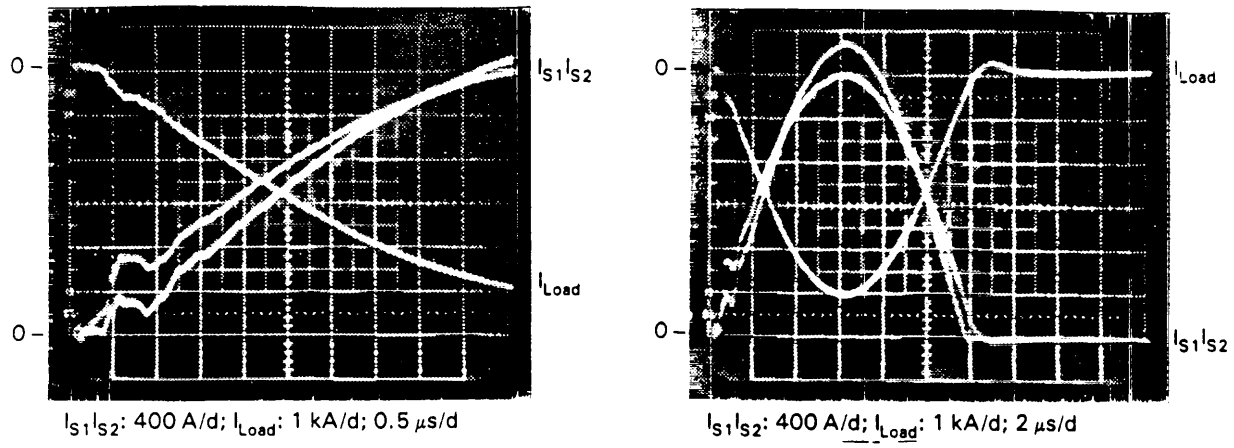

Fig. 9 Current-sharing between parallel connected thyratrons.

The characteristics of the auxiliary thyratron module are collected in Table 5.

Table 5

Auxiliary module characteristics

	U_{max} (V)	I_{max} (A)	Adjustment facility	Remarks
Cathode heater	8	50	variable transformer	Mains a.c.
Reservoir heater	8.5	10	variable transformer	Mains a.c.
Grid 1 priming	26	3	potentio-meter	Stabilized d.c.
Grid 2 bias	250	-	variable transformer	Non-stabilized d.c.
Grid 2 trigger pulse	2100	-	No	Voltage multiplier, fast thyristor, pulse transformer

4.3 Capacitors and magnetic elements

The HV energy-storage capacitor C_2 consists of thirty 80 nF units (LCC,F)connected in parallel. These are of the mixed dielectric

type (paper, polyethylene film, mineral-oil impregnation), built of bobbins with extended Al armatures, stacked in a polypropylene cylinder.

The LV smoothing choke L_1 has separate windings on the two columns of a window-frame core consisting of M6T35 material.

The 1:30 stepping-up transformer T_1 is a class B, resin-cast, two-column 10 kVA unit designed as a 50 Hz transformer taking into account the rectangular primary voltage waveform (Trasfor, CH). A 10 V tertiary winding is foreseen for voltage monitoring purposes. The total equivalent winding resistance, at 50 Hz and 20° C, with reference to the secondary has been specified not to exceed 150 Ω. An electrostatic screen is embedded between the internal LV primary and the HV secondary winding on each column.

The HV resonant charging choke L_2 is a two-column resin-cast unit with intermediate taps to adjust the desired charging time for a given capacitor C_2.

The HV air-core choke of the voltage-recovery circuit L_3 is made of six radial coils to approach a toroidal layout (Trasfor, CH). The dimensions of the choke (a 0.4 m side cube) are imposed by its position at the bottom of the pulser tank. To improve the voltage-recovery rate a Litz conductor has been used for this choke, which operates at 100 Hz with current pulses of 200 A peak and 300 μs duration.

4.4 HV transmission line

The converter solenoid is electrically connected, via a ceramic-insulated vacuum feedthrough, to the upper end of a 1 m long vertical sandwich line. The ~ 10 m long flexible transmission line from the pulser is connected to the bottom end of the sandwich line. The transmission line consists of ten 50 Ω polyethylene-insulated RG 213 U coaxial cables in parallel.

The design criteria of the pulse transmission line have been the following:

i) equivalent series impedance not exceeding 10% of that of the load;

ii) sufficient effective copper cross-section;

iii) minimum number of standard cables in parallel with highest possible characteristic impedance to facilitate approximate matching.

Figures 10a, b and c illustrate the solution adopted and show current and voltage waveforms at the output of the pulser. The matching line (ML) and $R_1 C_1$-$R_2 C_2$ networks are located in the pulser tank.

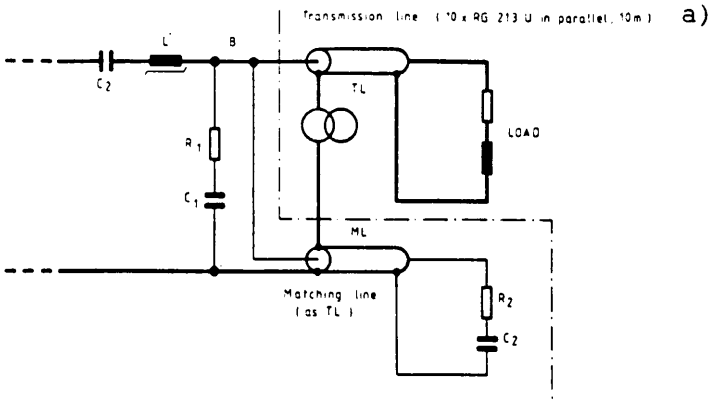

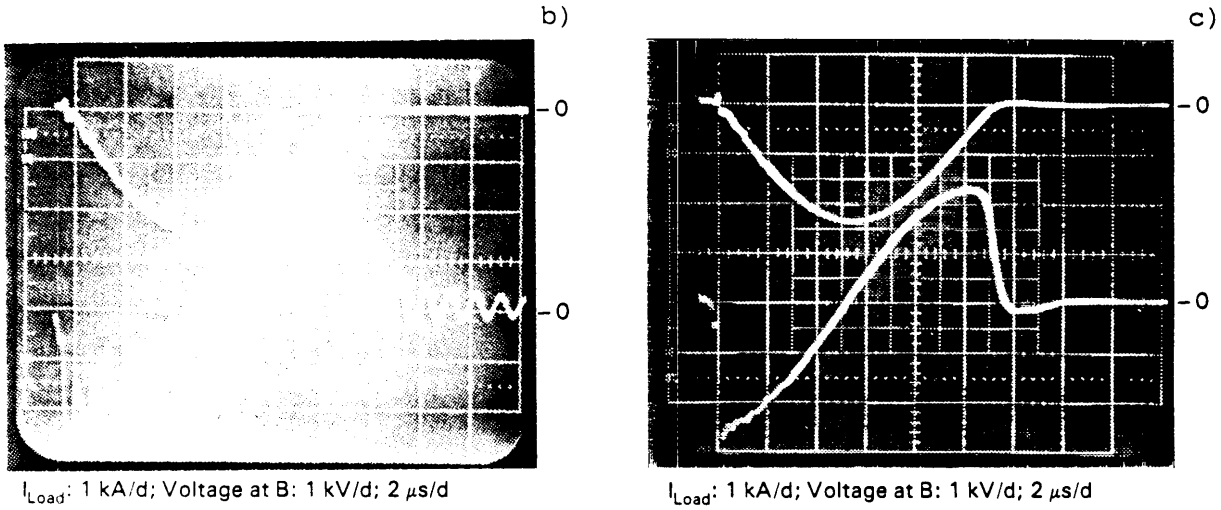

I_{Load}: 1 kA/d; Voltage at B: 1 kV/d; 2 μs/d

I_{Load}: 1 kA/d; Voltage at B: 1 kV/d; 2 μs/d

Fig. 10 a) Transmission line and matching components. Load current and voltage waveforms:
b) without and,
c) with matching line and components $R_1 C_1$, $R_2 C_2$.

4.5 Measuring devices

The load current as well as the individual anode currents and the current in the voltage recovery branch D_5, L_3 are monitored via fast current transformers located in the pulser tank.

The voltage potential at the anode end of the energy-storage capacitor C_2 is measured by means of a HV divider bought from industries, mounted on the external cylinder of the thyratron module (see Fig. 7). This signal is also used for pulse-to-pulse charging voltage stabilization. The maximum admissible cable distance from the voltage divider without signal deformation is ~ 3 m.

5. CONTROLS, TIMING, REGULATION, AND PROTECTIONS

5.1 Controls

The power supply is operated via the PS CAMAC computer interface network, using the standard protocol and timing sequence, and a local hybrid single transceiver module (STH).

The control protocol has the following exclusive actuation and acquisition states:

- OFF: The electromechanical power switches are open; the capacitors C_1 and C_2 are kept discharged; the reference signals to the regulation are set at zero; all timing and trigger pulses are inhibited.
- STAND-BY: The electromechanical switches are closed; the capacitors C_1 and C_2 are open circuited; all other conditions are unchanged.
- ON: The voltage of C_1 rises first to a pedestal (~ 50 V); then, after having started the inverter, it softly increases up to the preset value. The power supply operates as described in Section 3.
- RESET: Allows cancellation of the interlock signals once a fault condition has been cleared.

5.2 Timing

Two timing modes are foreseen:

i) external timing, via the computer interface preset counters;

ii) internal timing, via a fixed 100 Hz mains synchronized clock, or via an adjustable frequency pulse generator, or in a one-shot push-button mode.

The timing sequence is based on the following four pulses:

- FOREWARNING (FW) at -9 ms with respect to the next beam burst. This pulse turns on the inverter and starts the resonant charge of capacitor C_2. The charge of C_2 can be stopped after a fixed time interval or through the regulation once the preset voltage has been reached.

- WARNING (W) at -500 μs with respect to the beam. This pulse inhibits the inverter and starts the internal sequence to fire the thyratron within a given time window. The internal timing concerning the pulser is inhibited during the FW-W time interval.

- START (ST) at -5 μs with respect to the beam. This pulse triggers the thyratron and initiates the discharge of C_2; it must fall inside a 600 μs time window which includes the voltage recovery duration at C_2.

- MEASURE (M) is synchronous with the beam and is used to monitor the peak current in the solenoid, which is proportional to the voltage at C_2 at the ST pulse.

The functional block diagram of the timing electronics and the pulse sequence are shown in Fig. 11.

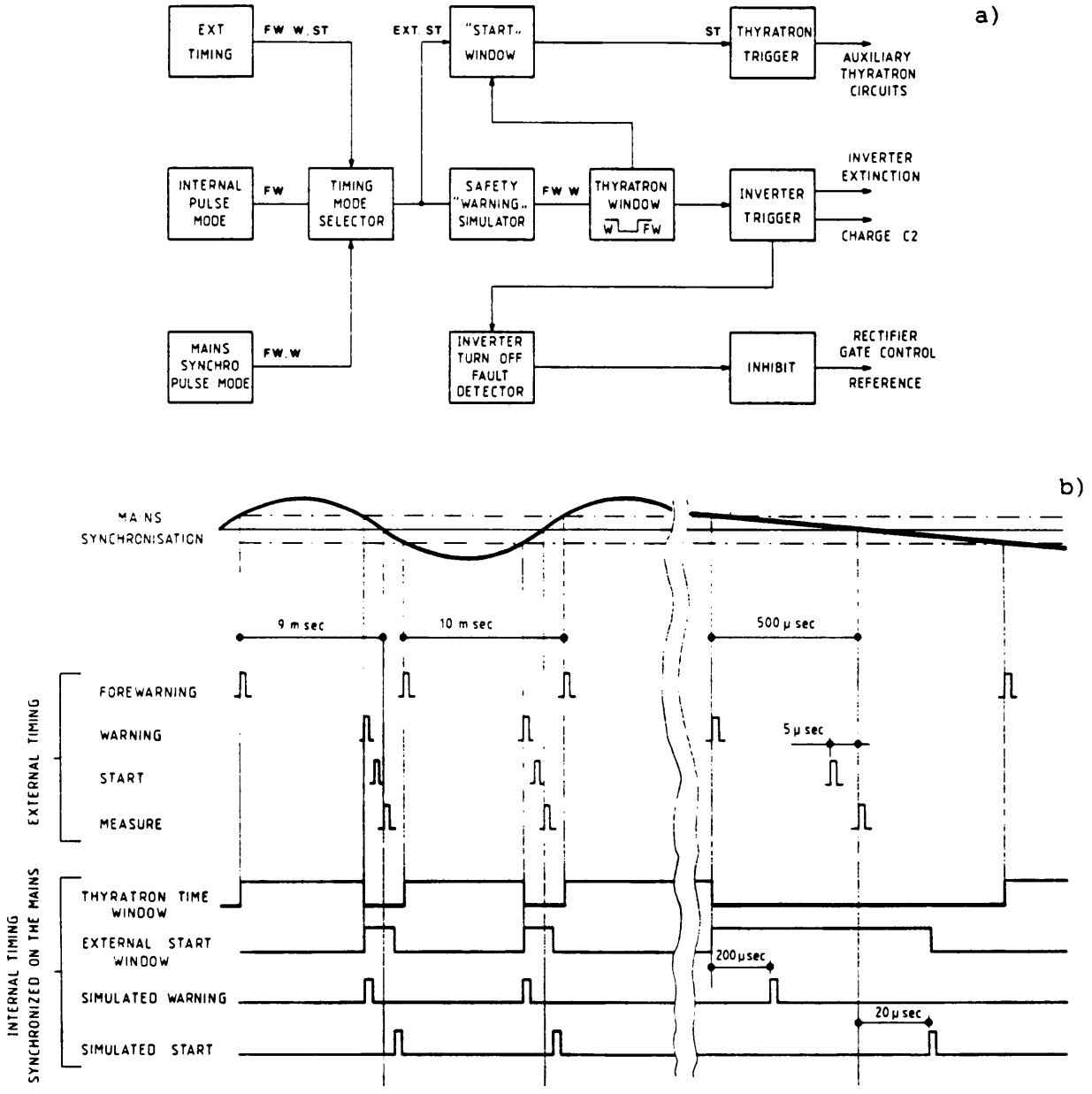

Fig. 11 Functional block diagram of
a) the timing electronics and,
b) the pulse sequence.

Internal safety pulses and interlock conditions are foreseen to counteract the accidental absence, doubling, or interchange of any of the above external pilot pulses. Owing to the internal safety pulses a timing sequence will always be completed in the right order, once initiated by an external FW pulse.

5.3 Regulation

The controlled variable is the voltage U_2 of the energy-storage capacitor C_2, on which depends the peak current in the collector solenoid. In practice the voltage U_1 is regulated since U_2 is a function of the recovery voltage U_{20} and of the voltage U_{10} of the buffer capacitor C_1 (see Appendix B).

The schematic layout of the regulation is represented in Fig. C1 (Appendix C). The charging and pulser circuit is considered to be a variable current sink, represented by a resistor R_{eq} in parallel with C_1. Depending on the operational conditions (U_1, U_2, pulse repetition frequency f) this resistor is assumed to vary between 10 Ω and 1000 Ω.

Independently of the actual value of R_{eq}, suitable correctors lead to satisfactory static and dynamic performances both of the internal current loop, which controls the charging current of C_1, and of the voltage loop, with stabilizes the voltage at C_1. The design of the power supply regulation is treated in more detail in Appendix C.

5.4 Protections

The protection and interlock circuits cope with any abnormal operating conditions or fault conditions, and in particular with those due to the possible misbehaviour of the external control system (e.g. timing) or of the active power components (thyristor rectifier, inverter, thyratron switch).

For example, back-firing of the thyratron will result in an overcurrent on the primary of the stepping-up transformer during the next resonant charging of C_2 owing to its lower initial voltage U_{20}. In this case the current will be interrupted by the forced-commutated inverter thyristors and the voltage at C_1 will be reset to the pedestal value and then ramped up to the reference value.

The power supply will return to normal operation without any action by the operations crew. The misbehaviour of the thyratron will be monitored and a WARNING signal given after a certain number of faults. Such an example is illustrated in Fig. 12.

The other protections and interlocks of the power supply produce either an OFF state (e.g. doors, thyristor rectifier faults, fuses, oil level in the pulser tank, earthing of capacitors C_1 and C_2, thyristor inverter fault, external faults) or a WARNING signal without further action, or a special recovery sequence similar to that of Fig. 12.

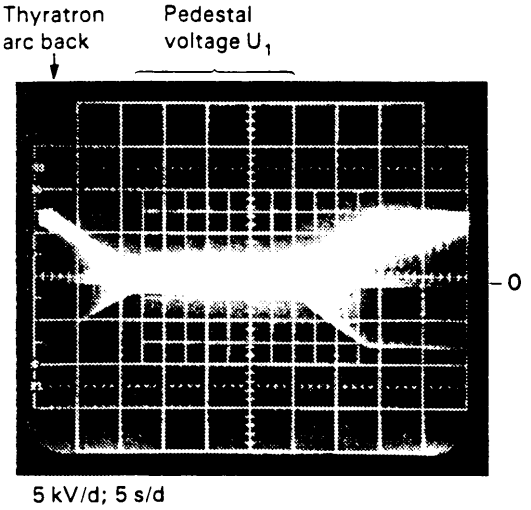

Fig. 12 Power supply protection in case of thyratron arc-back: voltage across thyratron.

6. CONSTRUCTIONAL LAYOUT

The power supply consists of two separate units, as shown in Fig. 2:

i) a charging cubicle (2.2 m^3), cooled by natural air convection, which includes the LV thyristor rectifier, LC filter and thyristor inverter, the stepping-up transformer, the HV rectifier and resonant choke, as well as the electronics and the auxiliary thyratron module;

ii) the pulser tank (1.3 m^3), silicon-oil filled, which contains the HV energy storage capacitor C_2, the thyratron switch module, the voltage-recovery choke and diodes, the curent- and voltage-measuring devices, the matching line, and RC networks.

The charging cubicle resembles other power electronics equipment while the unconventional pulser tank is illustrated in Fig. 13.

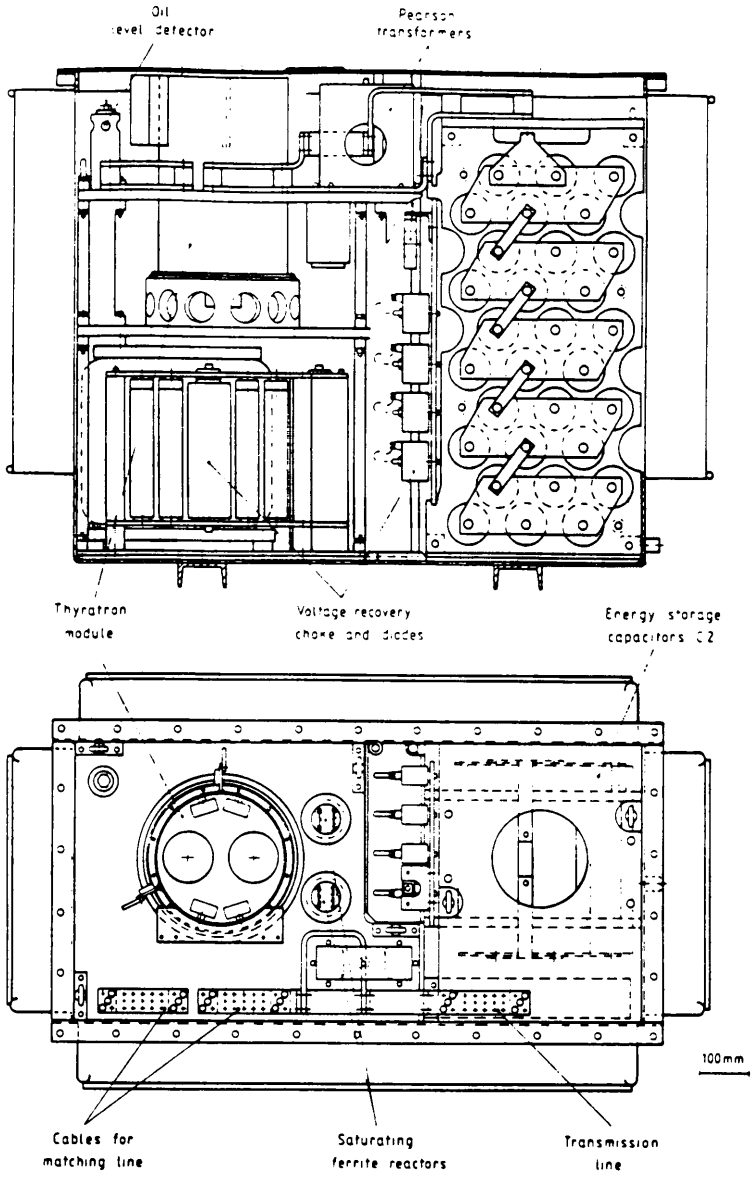

Fig. 13 Layout of pulser tank.

7. TEST RESULTS AND FIRST OPERATIONAL EXPERIENCE

First tests were done with electrons with a current peak of ~ 700 A [4] to verify the beam matching in the RF accelerating structure.

To facilitate beam operations the solenoid current signal is displayed in the local control room. The solenoid is at present pulsed at ~ 4000 A and gives an increase of the positron flux by a factor of ~ 3.

When testing the power supply some typical waveforms were recorded, which illustrate its operation and performance at 5 kA and 100 Hz; they are collected in Fig. 14.

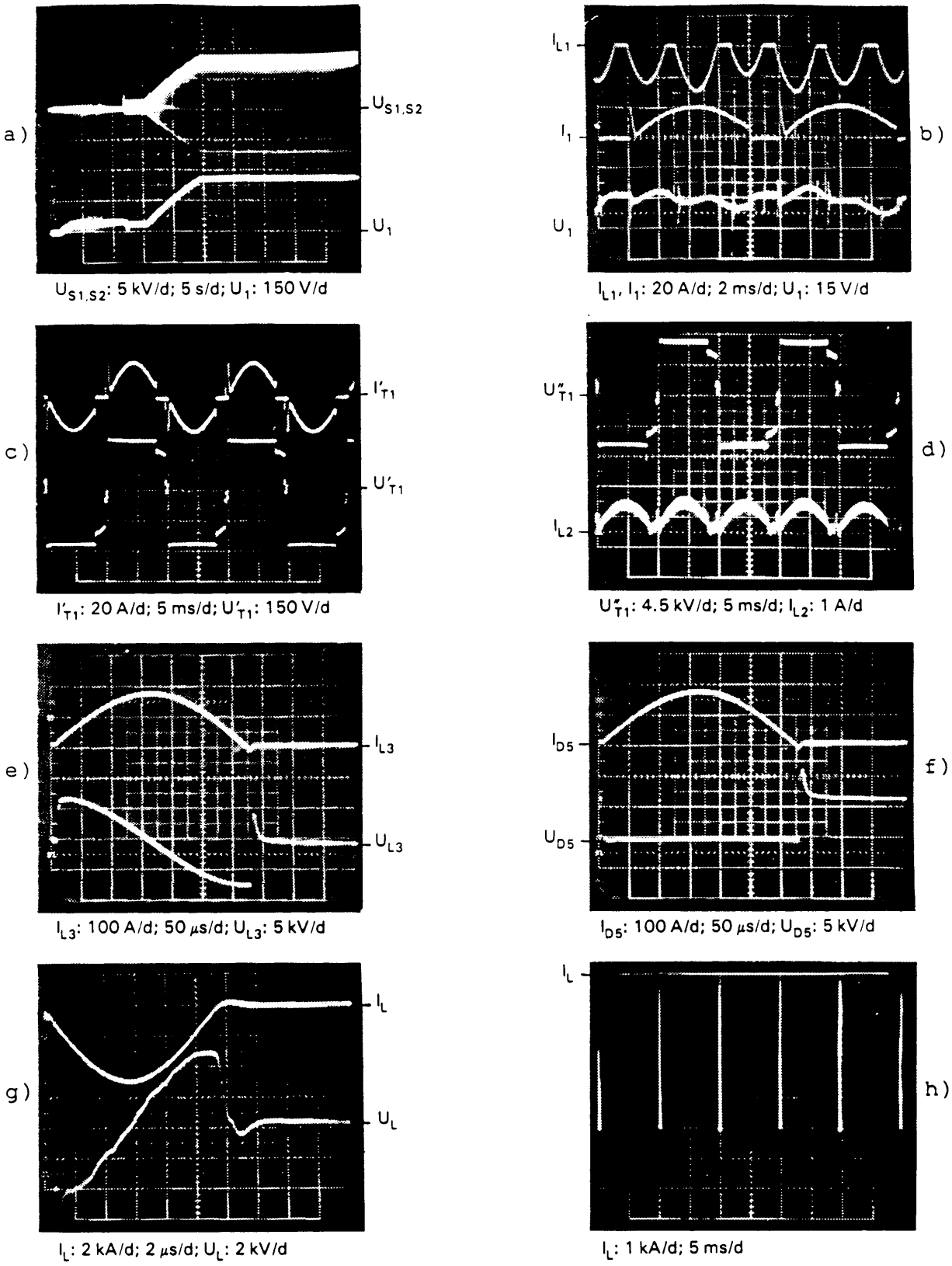

Fig. 14 Typical power supply waveforms (see Fig. 3):

a) Voltage at thyratron anode and at C_1 during a soft start.
b) Thyristor rectifier current, inverter current, and ripple voltage at C_1.
c) Primary current and voltage of stepping-up transformer
d) Voltage at secondary of transformer and current through the resonant choke L_2.
e) Current and voltage at the recovery choke.
f) Current and voltage at the recovery diodes.
g) Current and voltage at the collector solenoid.
h) Load current at 100 Hz pulse repetition frequency.

8. CONCLUSION

The circuit layout chosen reduces the energy stored in HV components. The use of a forced-commutated thyristor inverter on the primary of a 50 Hz stepping-up transformer allows effective protection in the case of a thyratron failure as well as fast active regulation of the charging voltage, as an alternative to the 'de-Q-ing' circuit solution.

The CX1528 (CX1526S) thyratron has been selected for this application. The investigation of its loading capability has demonstrated that, despite the reduction of the reverse voltage peak and du/dt in the circuit by the addition of appropriate components, reliable operation above 4.5 kA requires at present two tubes in parallel. Common heater and grid 2 bias power supplies are used for the two tubes. Separate d.c. supplies for grid 1 priming reduce the jitter at turn-on and allow optimization of the current sharing between tubes in the range of peak load current from 1 kA up to 6 kA.

Unwanted reflections and ringing could be eliminated by installing a complementary RC matching line in parallel with the pulse transmission line, to avoid having components in the highly radioactive converter target area.

The EMI problems have been overcome by a selective cable layout, by inserting suitable ferrite cores on all the cables, and by a careful earthing scheme.

The pulser has been installed separately from the HV charging section in a natural convection cooled transformer tank filled with silicon-oil. The two thyratrons have been mounted in parallel on an easily exchangeable switching module. The auxiliaries of both thyratrons are grouped in a common service module, located in the charging unit.

Acknowledgements

We should like to express our thanks to J. Madsen, LPI project leader, and to L. Coull, PO group leader, who entrusted this challenging work to us.

We acknowledge the contribution of several colleagues of the LPI, ML, and PO groups to the construction, installation and testing of the power supply and, in particular, the work of P. Grosjean*), who contributed to the development of the electronics and to the evaluation tests of the power circuit.

R. Bertolotto has been in charge of the construction of the converter solenoid itself and of the design of the target area.

Finally we should like to thank H. Menown, P. Maggs and L. Kettle of EEV (UK) for helpful discussions concerning the choice of the tube and for their participation in the investigation concerning the use of two tubes in parallel as a reliable solution for our application.

This report has been edited and typed by the Scientific Typing Service at CERN.

REFERENCES

[1] The LEP Injector Study Group, LEP Design Report, Vol. I: The LEP injector chain, CERN-LEP/TH/83-29 (1983).

[2] A. Fassó et al., Radiation problems in the design of the large electron-positron collider (LEP), CERN 84-02 (1984).

[3] G.H. Schröder and E.B. Vossenberg, High tension burst pulser for the electron extraction kickers of the CERN SPS, CERN-SPS/84-12 (ABT) (1984).

[4] D.I. Warner, First electron beams from the LEP injector linacs, CERN-PS/86-16 (1986).

*) At CERN on a temporary labour contract during part of the project.

APPENDIX A

Load current waveform

The load current consists of a train of damped half sine-wave pulses $i(t) = \hat{I}\, e^{-a\omega_2 t} \sin \omega_2 t$ of period T/k, when T is the pulse repetition period. Given the Fourier expansion of the current pulse train

$$i(t) = \hat{I}\left[\frac{a_0}{2} + \sum_n a_n \cos n\omega t + \sum_n b_n \sin n\omega t\right]$$

$$= \hat{I}\left[\frac{a_0}{2} + \sum_n c_n \sin (n\omega t + \varphi_n)\right]$$

with

$$c_n = (a_n^2 + b_n^2)^{1/2} \quad \text{and} \quad \varphi_n = \operatorname{arctg}\left(\frac{a_n}{b_n}\right),$$

the coefficients have been computed for general interest

$$\frac{a_0}{2} = \frac{1}{2\pi k} \frac{1}{(1+a^2)} (1 + e^{-a\pi})$$

$$a_n = \frac{1}{\pi k} \frac{[a^2 + 1 - (n^2/k^2)]}{\left\{a^2 + [1 + (n/k)]^2\right\}\left\{a^2 + [1 - (n/k)]^2\right\}} \left\{e^{-a\pi}\left[\cos \frac{n}{k}\pi - \frac{2a\, n/k}{[a^2 + 1 - (n^2/k^2)]} \sin \frac{n\pi}{k}\right] + 1\right\}.$$

$$b_n = \frac{1}{\pi k} \frac{[a^2 + 1 - (n^2/k^2)]}{\left\{a^2 + [1 + (n/k)]^2\right\}\left\{a^2 + [1 - (n/k)]^2\right\}} \left\{e^{-a\pi}\left[\sin \frac{n}{k}\pi + \frac{2a\, n/k}{[a^2 + 1 - (n^2/k^2)]} \cos \frac{n\pi}{k}\right] + \frac{2a\, n/k}{[a^2 + 1 - (n^2/k^2)]}\right\}$$

These Fourier coefficients are shown in Fig. A1 for a = 0.2116.

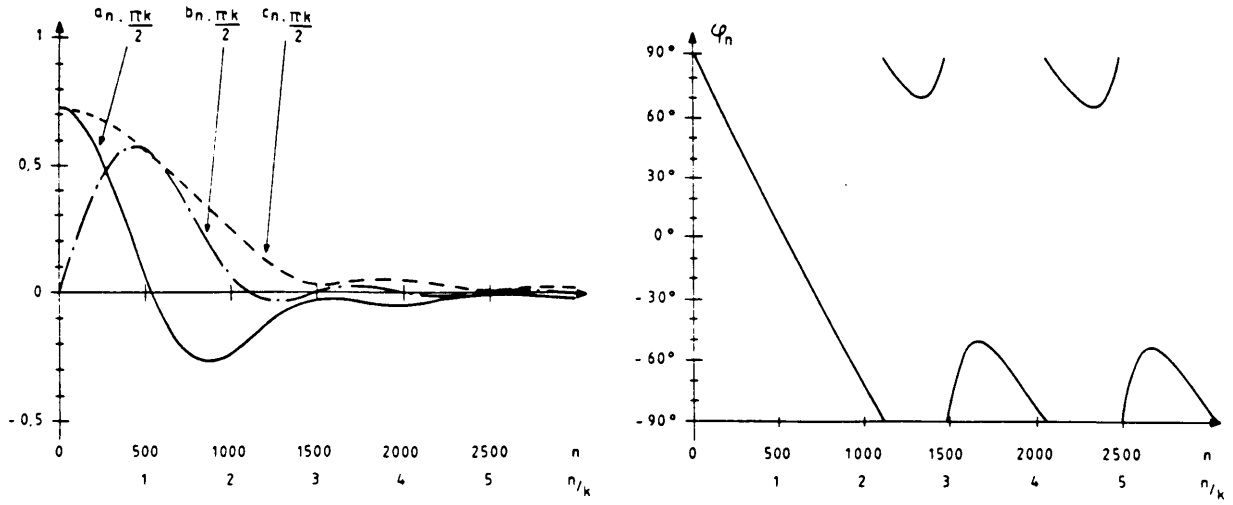

Fig. A1 Fourier coefficients; a = 0.2116.

When a = 0 (no damping) the Fourier coefficients become

$$\frac{a_0}{2} = \frac{1}{\pi k}$$

$$a_n = \frac{k}{\pi} \frac{1}{(k^2 - n^2)} \left[\cos\left(\frac{n\pi}{k}\right) + 1\right]$$

$$b_n = \frac{k}{\pi} \frac{\sin\left[(n/k)\pi\right]}{(k^2 - n^2)} \ .$$

The Fourier coefficients for a = 0 are shown in Fig. A2.

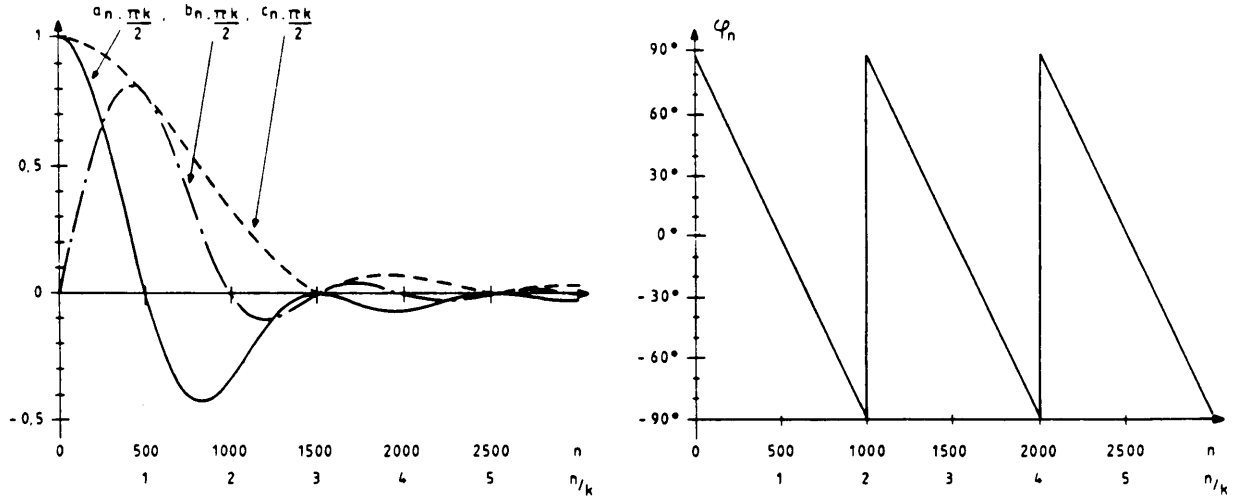

Fig. A2 Fourier coefficients; a = 0.

APPENDIX B

Power circuit analysis

The power circuit is schematically represented in Fig. B1.

It is assumed that at $t = 0$ all switches are open and the operating cycle is divided into four intervals:

1. Switch S_a is closed until the buffer capacitor C_1 is charged by the source U_0 to its initial value $U_{10} = U_0$. In practice, switch S_a is permanently closed and C_1 connected to the rectifier via R_1, L_1; the real voltage at C_1 during operation is represented in Fig. 14b.

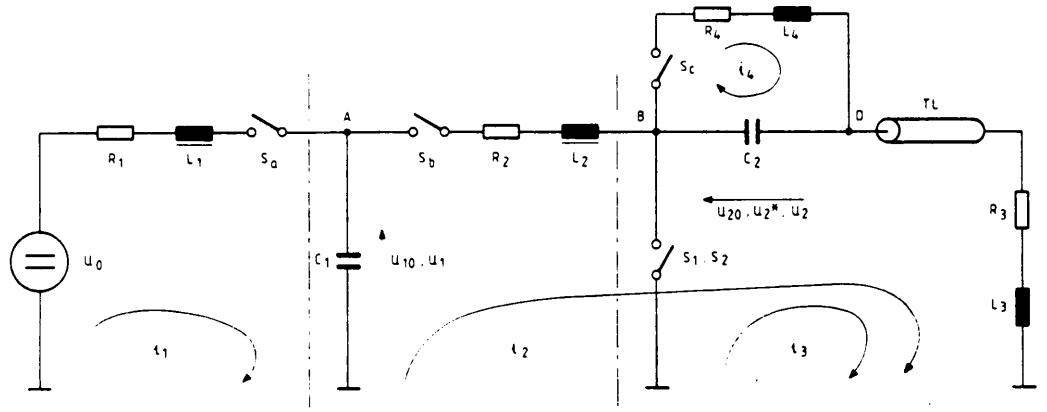

Fig. B1 Schematic diagram of power circuit referred to the primary of the stepping-up transformer.

2. Switch S_a is opened and resonant charging of C_2 is started from an initial voltage U_{20} by closing S_b.

The following analytical expressions are derived:

i) The charging current is

$$i_2(t) = \frac{(U_{10} - U_{20})}{\omega_2 L} e^{-\delta_2 t} \sin \omega_2 t ,$$

where

$$\omega_0 = \frac{1}{(LC)^{1/2}} , \quad Q = \frac{\omega_0 L}{R} , \quad \xi = \frac{R}{2}\left(\frac{C}{L}\right)^{1/2} ,$$

$$\delta_2 = \xi\omega_0 = \frac{R}{2L} , \quad \omega_2 = (\omega_0^2 - \delta_2^2)^{1/2} ,$$

with

$$R = R_2 + R_3 , \quad C = \frac{C_1 C_2}{C_1 + C_2} = \frac{n}{(n+1)} C_2 , \quad L = L_2 + L_3 ,$$

ii) The mean value of the charging current is

$$\bar{i}_2 = \frac{\omega_2 C_2 U_2}{\pi} (1-\alpha) = i_0 (1-\alpha) ,$$

where α is the ratio between initial voltage U_{20} and charging voltage U_2

$$\alpha = \frac{U_{20}}{U_2} , \quad i_0 = \frac{U_2 C_2}{T_2/2} ,$$

and $T_2/2 = \pi/\omega_2$ is the resonant charging time.

iii) The effective value of the charging current is

$$i_{2\,eff} = i_0 \frac{\pi}{2} \left(1 + \frac{\delta_2^2}{\omega_2^2}\right)^{1/2} \cdot (1-\alpha) \left[\frac{[(1/\pi)(\omega_2/\delta_2)\beta_1\beta_2]^{1/2}}{\beta_1}\right] ,$$

where

$$\beta_1 = 1 + e^{-(\delta_2/\omega_2)\pi} \quad \text{and} \quad \beta_2 = 1 - e^{-(\delta_2/\omega_2)\pi} .$$

iv) The final voltage of C_2 is

$$U_2 = U_{20} + \Delta U_2 = U_{20} + (U_{10} - U_{20}) \frac{n}{(n+1)} \beta_1 .$$

v) The initial voltage U_{10} required to charge C_2 at U_2 is

$$U_{10} = U_2 \frac{1 + \alpha[n\beta_1/(n+1) - 1]}{[n/(n+1)]\beta_1} .$$

vi) The mean input power is

$$P_0 = U_{10}\,\bar{i}_2 \ .$$

These relations are represented in Fig. B2 and permit designing the power circuit for the case where the resistance R (with reference to the HV side) assumes values between 100 and 300 Ω.

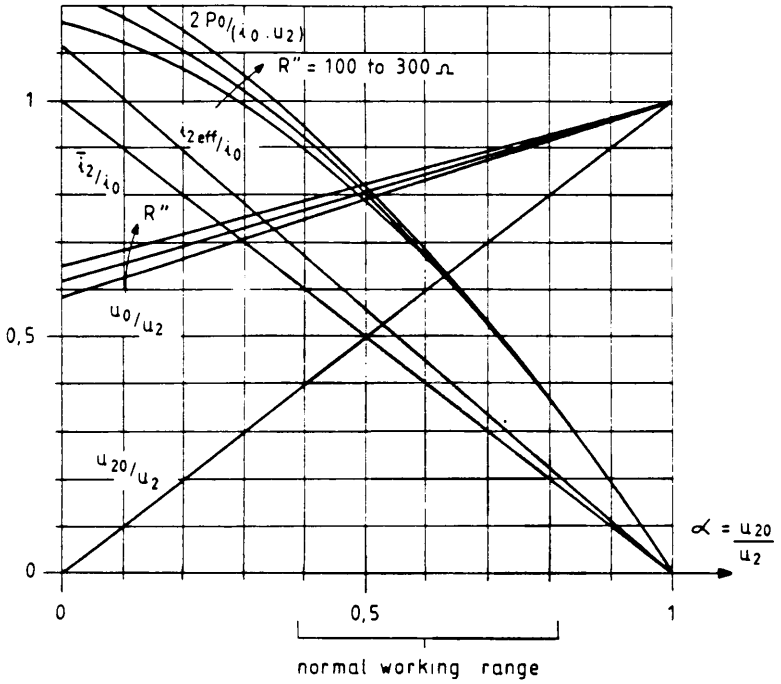

Fig. B2 Diagrams of circuits parameters as a function of the resistance R" and the voltage recovery ratio α.

3. At the end of the resonant charging interval, switch S_b opens and switch S_1, S_2 is closed. Node B is then connected to earth potential and node D assumes a potential $-U_2$.

The current flowing through the load is

$$i_3(t) = \frac{U_2}{\omega_3 L_3}\, e^{-\delta_3 t} \sin \omega_3 T \ ,$$

where

$$\delta_3 = \frac{R_3}{2L_3} \qquad \text{and} \quad \omega_3 = \left(\frac{1}{L_3 C_2} - \delta_3^2\right)^{1/2} \ .$$

The peak load current is

$$\hat{i}_3 \simeq \frac{U_2}{\omega_3 L_3} e^{-\delta_3 \pi/2\omega_3} .$$

The voltage at D varies according to the expression

$$U_3(t) = -U_2 \left(\cos \omega_3 t + \frac{\delta_3}{\omega_3} \sin \omega_3 t\right) e^{-\delta_3 t} ,$$

reaching the value $U_2^* = U_2 e^{-\delta_3 \pi/\omega_3}$ at $t = \pi/\omega_3$.

4. Once the switch S_1, S_2 has de-ionized after zero crossing of $i_3(t)$, the voltage at B jumps to $-U_2^*$. Then switch S_c is closed and the voltage at C_2 swings from $-U_2^*$ to the recovery voltage U_{20} according to the expression

$$U_4(t) = -U_2^* \left(\cos \omega_4 t + \frac{\delta_4}{\omega_4} \sin \omega_4 t\right) e^{-\delta_4 t}$$

where

$$\delta_4 = \frac{R_4}{2L_4} \quad \text{and} \quad \omega_4 = \left(\frac{1}{L_4 C_2} - \delta_4^2\right)^{1/2}$$

The current in the recovery circuit is

$$i_4(t) = \frac{U_2^*}{\omega_4 L_4} e^{-\delta_4 t} \sin \omega_4 t .$$

The final recovery voltage and the peak recovery current are

$$U_{20} = U_2^* e^{-\delta_4 \pi/\omega_4}$$

$$\hat{i}_4 \simeq \frac{U_2^*}{\omega_4 L_4} e^{-\delta_4 \pi/2\omega_4} .$$

APPENDIX C

Power supply regulation

In Fig. C1 the power supply voltage (U_1) and current (i_1) regulation have been designed to cope with the low source impedance (R_1) and with the pulse frequency dependent load impedance (R_{eq}).

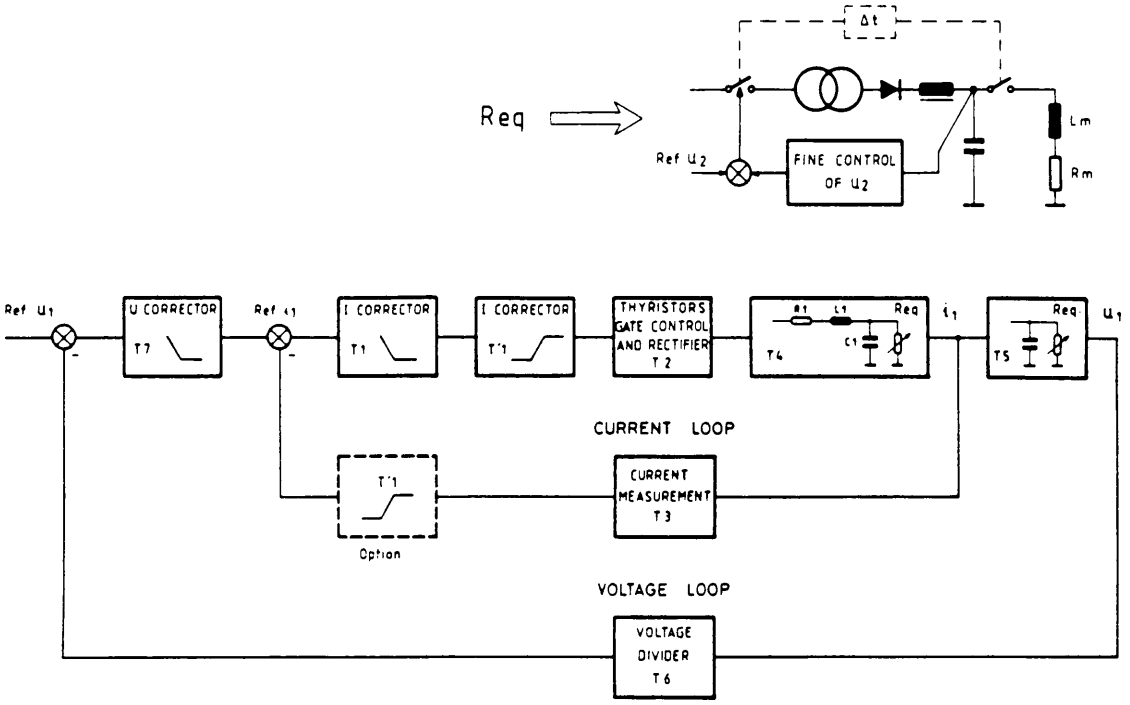

Fig. C1 Power supply regulation loops.

1. Current loop

The basic approximate transfer functions are

$$(T_2 T_3)T_4 = \frac{7.6 \times 10^3}{(s + 470)} \times$$

$$\left[\frac{1+R_{eq}C_1 s}{R_1+R_{eq}} \; \frac{1}{1 + \frac{2R_{eq}}{R_1+R_{eq}}\left[\frac{R_1}{2}\left(\frac{C_1}{L_1}\right)^{1/2} + \frac{1}{2R_{eq}}\left(\frac{L_1}{C_1}\right)^{1/2}\right]\frac{s}{\omega} + \frac{R_{eq}}{R_1+R_{eq}}\frac{s^2}{\omega^2}}\right]$$

where $R_1 = 0{,}3\ \Omega$, $L_1 = 12{,}5$ mH, $C_1 = 25$ mF, $10\ \Omega \leq R_{eq} \leq 1000\ \Omega$, $\omega = 18\pi$ Hz.

Two correctors and an attenuator have been added:

$$0.14 T_1 T_1' = 0.14 \left(\frac{s + 10^2}{10s} \right) \left(\frac{10^4 + 10^2 s}{10^3 + s} \right)$$

and the diagrams shown in Fig. C2 have been obtained for the open-loop transfer function T_8 and closed-loop transfer function T_9.

The design option of placing the corrector T_1' in the feedback has been computed and tested to achieve a higher damping factor if needed.

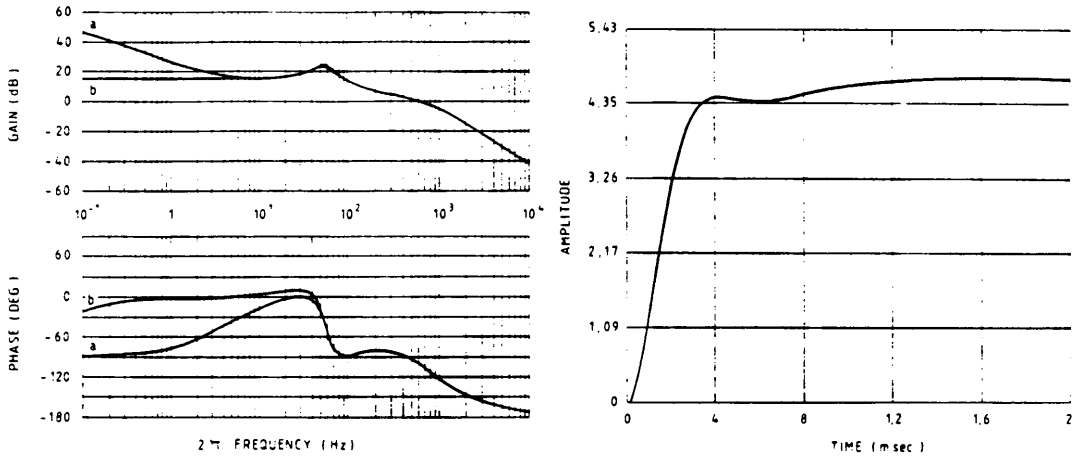

Fig. C2 Frequency response of current open loop transfer function (T_8) and step response of current closed loop transfer function (T_9); R_{eq} = 10 Ω (a) and 1000 Ω (b).

2. Voltage loop

Given the current transfer function T_9 as well as the voltage loop transfer functions $T_6 = 1/30$ and $T_5 = R_{eq}/(1 + R_{eq}C_1 s)$, a corrector $T_7 = 10(1+s)/s$ has been added and the open-loop and closed-loop voltage transfer function diagrams shown in Fig. C3 have been obtained.

Finally the regulation has been tested on the power supply with different pulse repetition frequencies and taking into account all possible operational situations. It performed satisfactorily and only minor gain adjustments were required to optimize the transient behaviour.

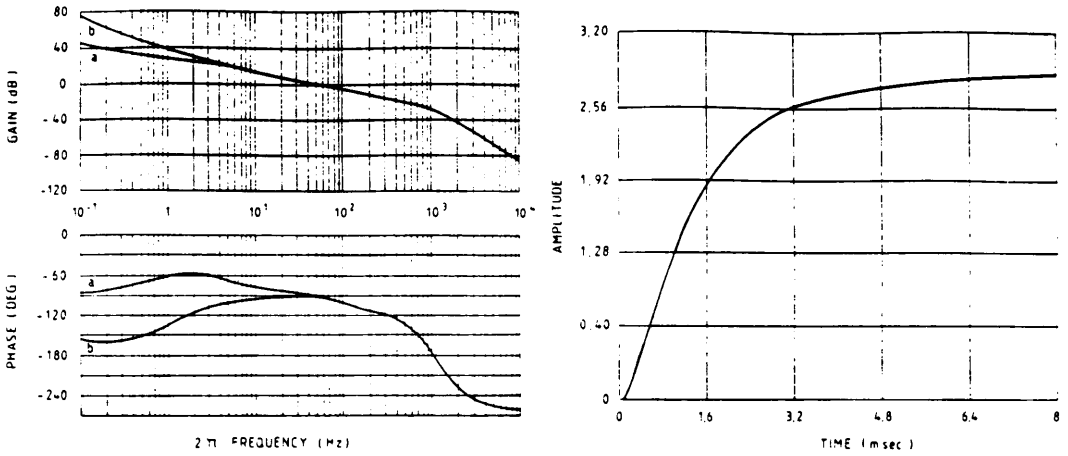

Fig. C3 Frequency response of voltage open loop transfer function (T_{10}) and step response of voltage closed loop transfer function (T_{11}); R_{eq} = 10 Ω (a) and 1000 Ω (b).

PS DIVISION REPORTS

January - December, 1988

CERN/PS 88-01 (PO)	The 6kA, 10kV, 100 Hz Power Supply and Pulser for the Collecting and Focusing Solenoid of the e^-e^+ Converter in the CERN LEP Pre-Injector.	J.P. Royer F. Volker
CERN/PS 88-02 (OP)	Statistics of PS Operation, 1987.	G. Azzoni
CERN/PS 88-03 (DL)	PS Division Reports 1987.	S.L. Neboux
CERN/PS 88-04 (CO)	Contribution to the Annual Report 1987 - Controls Group.	F. Perriollat
CERN/PS 88-05 (AR)	On the Feasibility of Antideuteron Production and Storage at CERN (Paper presented at the Symposium on the Production and Investigation of Atomic Antimatter, Karlsruhe, 30.11-2.12.87.)	C.D. Johnson T.R. Sherwood
CERN/PS 88-06 (OP)	Measurements and Surprises with H-minus Ions. (IVth LEAR Workshop, Villars-sur-Ollon, Switzerland, 6.-13.9.88.)	D. Manglunki
CERN/PS 88-07 (LP)	Parameters of the LEP Injector Linacs.	D.Blechschmidt D.J. Warner
CERN/PS 88-08 (PA)	Particle Acceleration by RF Pulse Compression.	R. Cappi
CERN/PS 88-09 (AR)	High-Power, High-Current Pseudospark Switches (Paper presented at the XIIIth Int.Symposium on Discharges and Electrical Insulation in Vacuum, Paris, 1988.)	E. Boggasch H. Riege
CERN/PS 88-10 (DL)	Workshop on a Lead-Ion Linac for the CERN Accelerator Complex (CERN, 25-26.5.87.)	U.Tallgren
CERN/PS 88-11 (AR)	Absolute and High Precision Measurements of Particle Beam Parameters at CERN Antiproton Storage Ring LEAR using Spectral Analysis with Correction Algorithms. (Presented at the EUSIPCO-88, Grenoble, September 1988.)	E. Asséo J. Bengtsson M. Chanel
CERN/PS 88-12 (CO)	A Fault Diagnosis Expert System for CERN using KEE. (Invited talk for the SEAS - Share European Association - Spring Meeting, Davos, 18-22.4.1988.)	I. Alarcon E. Malandain S. Pasinelli P. Skarek
CERN/PS 88-13 (DL)	End Effects in Quantum Bremsstrahlung. (Submitted to Particle Accelerators.)	J.S. Bell M. Bell
CERN/PS 88-14 (ML)	Trapping of Ions in the EPA Electron Beam: Stability Conditions and Diagnosis.	A. Poncet
CERN/PS 88-15 (AR)	Antiproton Intensity Limitations. (Symposium on the Production and Investigation of Atomic Antimatter, Karlsruhe, Nov. 30-Dec. 2, 1987.)	B. Autin
CERN/PS 88-16 (AR) CERN/SPS 88-10 (DI)	The CERN $p\bar{p}$ Collider (to be published in World Scientific Series on Directions in High Energy Physics, Vol. 4).	L. Evans E. Jones H. Koziol
CERN/PS 88-17 (AR)	Model Measurements for New Accelerating Techniques. (Invited contribution to the Workshop on Pulse Power Techniques, Erice, Italy, 5-9 March 1988.)	S. Aronson(BNL) H. Haseroth J. Knott W. Willis
CERN/PS 88-18 (AR)	Closed Orbit Correction of the CERN Antiproton Collector Ring (EPAC, Rome, 7-11 June, 1988.)	M. Martini L. Rinolfi
CERN/PS 88-19 (LP)	Positron Production for Particle Accelerators. (Symposium on the Production and Investigation of Atomic Antimatter, Karlsruhe, 30.11-2.12.87.)	K. Hübner
CERN/PS 88-20 (ML)	The Vacuum Systems of the LEP Injector Chain. (Topical Conference on Vacuum Design of Advanced and Compact Synchrotron Light Sources, Brookhaven, 16-18 May 1988.)	A. Poncet
CERN/PS 88-21 (AR)	Calculation of Protonium Production Rate from Corotating Beams of $p\bar{}$ and H^- in LEAR. (EPAC, Rome, 7-11 June 1988.)	R. Giannini
CERN/PS 88-22 (LP)	Status Report on the LEP Pre-Injector (LPI) and the Proton Synchrotron (PS) as e^+e^- Accelerator. (EPAC, Rome, 7-11 June 1988.)	S. Battisti et al.
CERN/PS 88-23 (LP)	Measurements and Analysis of Collective Effects in the LEP Electron Positron Accumulator (EPA). (EPAC, Rome, 7-11.6.88.)	S. Bartalucci et al.
CERN/PS 88-24 (AR)	PS Beam Dynamics Activities (Lugano 1988, to be published in Beam Dynamics News Letters).	B. Autin Editor
CERN/PS 88-25 (AR)	Design and Performance of the AC Stack Core Cooling System.(EPAC, Rome, 7-11 June 1988.)	J. Bosser P. Bramham C. Metzger C.S. Taylor

CERN/PS 88-28 (HI)	Strategies for Longitudinal Painting in the EAF Booster at Injection. (EPAC, Rome, 7.-11.6.88.)	E. Gianfelice H. Schonauer
CERN/PS 88-29 (HI)	Accelerating and Separating Mixed Beams of Ions with Similar Charge to Mass Ratio in the CERN PS Complex. (EPAC, Rome,7.-11.6.88.)	E. Brouzet et al.
CERN/PS 88-30 (DL)	Future of Heavy Ion Programme at CERN. (Invited talk at the Int.Conference on Physics and Astrophysics of Quark-Gluon Plasma, Bombay, 8.-12.2.88.)	H. Haseroth
CERN/PS 88-31 (RF)	Low Frequency Ferrite Cavities. (EPAC, Rome, 7-11.6.1988.)	A. Susini
CERN/PS 88-32 (RF)	A Preliminary Study of a Voltage Multiplying Structure for Electron Acceleration. (EPAC, Rome, 7-11.6.1988.)	A. Fiebig G. Nassibian Ch. Schieblich
CERN/PS 88-33 (RF)	A Radiofrequency Pulse Compressor for Square Output Pulses. (EPAC, Rome, 7-11.6.1988.)	A. Fiebig Ch. Schieblich
CERN/PS 88-34 (AR)	A z-Pinch Plasma Lens for Focusing High-Energy Particles in an Accelerator. (EPAC, Rome, 7-11 June 1988.)	B. Autin et al.
CERN/PS 88-35 (OP)	Knowledge Engineering Methods for Accelerator Operation. (EPAC, Rome, 7-11.6.88.)	E. Malandain S. Pasinelli P. Skarek
CERN/PS 88-36(CO-LPI)	Modulation of the Lepton Production for the CERN LEP Pre-injector. (EPAC, Rome, 7-11.6.88.)	G.P. Benincasa et al.
CERN/PS 88-37 (ML)	EPA Beam Vacuum Interaction Ion Clearing System. (EPAC, Rome, 7-11.6.88.)	E. Caspers J.P. Delahaye J.C. Godot K. Hubner A. Poncet
CERN/PS 88-38 (AR)	LEAR Beam Stability Improvements using FFT Analysis. (EPAC, Rome, 7-11.6.88.)	E. Asséo J. Bengtsson M. Chanel
CERN/PS 88-39 (LP)	Beam Loading Analysis of a Transformer-Coupled RF Cavity. (EPAC, Rome, 7-11.6.88.)	S. Bartalucci R. Garoby A. Riche A. Susini
CERN/PS 88-40 (LP)	Closed Orbit Distortions and their Corrections in the 600 MeV Electron-Positron Accumulator at LEP. (EPAC, Rome, 7-11.6.88.)	S. Battisti D. Brandt H. Kugler J.P. Potier A. Verdier
CERN/PS 88-41 (PA)	The Magnet System of the Electron Positron Accumulator (EPA). (EPAC, Rome, 7-11.6.88.)	O. Cornuet

CERN/PS 88-42 (PA)	New Electrostatic Pick-ups for the PS. (EPAC, Rome, 7-11.6.88.)	J. Durand J. Gonzalez E. Schulte M. Thivent
CERN/PS 88-43 (AR)	Performance of the CERN Antiproton Accumulator Complex. (EPAC, Rome, 7.-11.6.1988.)	B. Autin et al.
CERN/PS 88-44 (AR)	The CERN Antiproton Collector Ring. (EPAC, Rome, June 7-11, 1988.)	B. Autin et al.
CERN/PS 88-45 (AR) CLIC Note 68	The CLIC Project and the Design for an e^+e^- Collider. (Lecture given at the Int.School on Electromagnetic Radiation and Particle Beams: Physics and Applications, Varenna, Italy, June 1988.)	S. van der Meer
CERN/PS 88-46 (AR)	Nonlinear Beam Behaviour in the CERN Antiproton Collector. (EPAC, Rome, 7.-11.6.88.)	P. Krejcik
CERN/PS 88-47 (AR) CLIC Note 67	Design for a Practical, Low-emittance Damping Ring. (EPAC, Rome, June 7-11, 1988.)	P. Krejcik
CERN/PS 88-48 (AR)	Correction of Sextupolar Beam Envelope Distortion. (Paper presented at the ICFA Workshop on Beam Dynamics, Lugano, 11-16.4.88.)	B. Autin
CERN/PS 88-49 (AR)	Dynamic Aperture and Invariance Behaviour in the CERN Antiproton Collector. (Paper presented at the ICFA Workshop on Beam Dynamics, Lugano, April 11-16, 1988.)	P. Krejcik
CERN/PS 88-50 (AR)	Second Order Tune Shift in a Compensated Super Cell. (Paper presented at the ICFA Workshop on Beam Dynamics, Lugano,11-16.4.88.)	B. Autin F. Willeke
CERN/PS 88-51 (DL)	Planning and Proposals for the CERN Heavy Ion Injector. (Conf. for Production of and Physics with Highly Stripped Ions, Grenoble, September 1988.)	H.Haseroth
CERN/PS 88-52 (AR)	High-Power Pseudospark and BLT Switches. (Paper published in IEEE Transactions on Plasma Science, Vol. 16 No.2, April 1988.)	E. Boggasch et al.
CERN/PS 88-53 (AR)	Fast Polarization Changes in Ferroelectrics and their Applications in Accelerators. (To be submitted for publication to Nuclear Instruments and Methods in Physics Research.)	H. Gundel J. Handerek H. Riege E.J.N. Wilson K. Zioutas
CERN/PS 88-54 (AR)	Fast Polarization Changes in PZT Ceramics by High Voltage Pulses. (Presented at 1st European Conference on Applications of Polar Dielectrics and Int.Symposium on Applications of Ferroelectrics, Zurich, August 1988.)	H. Gundel J. Handerek H. Riege E.J.N. Wilson K. Zioutas
CERN/PS 88-55 (AR)	A Proposal to use a Plasma Lens to achieve a 12 mm Spot at the End of CLIC.	B. Fedele E.J.N. Wilson
CERN/PS 88-56 (CO)	Accelerator Controls. (Lecture given at the 1988 CERN School of Computing, Queens College, Oxford, August 1988.)	F.Perriollat
CERN/PS 88-57 (DL)	Quantum Bremsstrahlung: report to Workshop on Linear Colliders.	M. Bell J.S. Bell
CERN/PS 88-58 (RF)	Kickers and Septa at the PS Complex, CERN. (Paper presented at the Magnet Workshop, TRIUMF, Vancouver, Canada, 3.-5.10.88.)	D. Fiander K.D. Metzmacher P. Pearce
CERN/PS 88-59 (AR/OP)	Beam Impedance Measurements using the Coaxial Wire Method. (Paper presented at the Workshop on Impedances and Current Limitations, ESRF-Grenoble, 17-18 October, 1988).	F. Caspers
CERN/PS 88-60 (AR)	Diagnostics with Schottky Noise.(Joint US-CERN School on Beam Observation, Diagnosis and Correction, Capri, October 1988.)	S. van der Meer
CERN/PS 88-61 (LP)	Linear Collider Work at CERN. (Invited talk at the XXIV Int.Conf. on High Energy Physics, Munich, 4.-10.8.88.)	K. Hübner
CERN/PS 88-62 (HI-LP)	New and Proposed Linacs at CERN : the LEP (e^+/e^-) Injector and the SPS Heavy Ion (Pb) Injector. (Paper presented at the 1988 Linear Accelerator Conference, Williamsburg, Virginia, U.S.A., October, 1988).	D.J. Warner
CERN/PS 88-63 (HI)	Heavy Ion Acceleration using Drift-Tube Structures with Optimised Focusing. (Paper presented at the 1988 Linear Accelerator Conference, Williamsburg, Virginia, U.S.A., October 1988).	D.J. Warner
CERN/PS 88-64 (HI)	Integral Protection and Fault Diagnostics for Interconnected Timing Systems in a Large Accelerator Complex. (Paper presented at the Europhysics Conference on Control Systems for Experimental Physics, Villars-sur-Ollon, Vaud, Switzerland, 28 September - 2 October 1987).	J. Knott H. Nettleton
CERN/PS 88-65 (AR)	Fast Polarization Changes in Ferroelectrics	H. Gundel

CERN/PS 88-68 (ML)	Industry and the Accelerator Vacuum Field : a Long Tradition of Successful Collaboration. (CERN Accelerator School, Salamanca, 19-30.9.88.)	A. Poncet
CERN/PS 88-69 (AR)	Theoretical Antiproton Yields for the AAC	N.J. Walker
CERN/PS 88-70 (AR)	A Low-Pressure Hollow Cathode Switch triggered by a Pulsed Electron Beam emitted from Ferroelectrics. (Submitted for publication in Applied Physics Letters.)	H. Gundel J. Handerek H. Riege K. Zioutas
CERN/PS 88-71 (PA)	Commande adaptative à modèle de référence de systèmes discrets.	J.L. Gonzalez
CERN/PS 88-72 (HI)	Design of the Preinjector for the CERN RFQ2 Project.	Ch. Hill K. Prelec M. Weiss
CERN/PS 88-73 (PA)	A New Type of Position Sensitive Electron Multiplier.	V. Agoritsas K. Kuroda Ch. Nemoz
CERN/PS 88-74 (AR)	Electromagnetic Properties of Steel-Fiber Reinforced Concrete in the RF and Microwave Range.(Paper to be presented at the 8th Int. Symposium and Technical Exhibition on Electromagnetic Compatibility, Zurich, 7-9.3.89.)	F. Caspers V. Hansen D. Stein
CERN/PS 88-75 (PA)	A New Beam-Profile Monitor for very Low Energy Antiprotons Beams.	V. Agoritsas K.J. Kuroda Ch. Nemoz
CERN/PS 88-76 (OL)	Radial Transmission Lines. (Invited talk at Switched Power Workshop, Shelter Island, NY, 16-21.10.8.)	H. Haseroth et al.
CERN/PS 88-77 (OP/PA)	Simulation of the PS Slow Extraction 62 with the MAD Program.	F. Galluccio T. Risselada C. Steinbach M. Tanaka
CERN/PS 88-78 (OP)	Offices Local Area Network at the PS Division.	A. Pace

See (lists)ps-reports-89